Check for updates

ChemCatChem

Research Article
doi.org/10.1002/cctc.202501122

Chemistry Europe
European Chemical Societies Publishing

www.chemcatchem.org

High-Pressure Electrocatalytic Reduction of CO_2 to CO Under Realistic Conditions

Noë I. Watson,[a, b] Charlotte von Quadt,[a, b] Stanislav Molodtsov,[b] Lukas Balk,[b] Bart van den Bosch,[b] and Gadi Rothenberg*[a]

We study the key factors governing the high-pressure electrochemical reduction of CO_2 to CO using commercial silver electrodes. Voltammetry and electrolysis results, combined with X-ray diffraction and microscopy analyses, show that the applied current density is the most important parameter. When this is doubled from 150 to 300 mA/cm$^2_{geo}$, the CO yield goes down drastically, and more hydrogen is produced at the cathode. At the lower current density (150), the hydrogen production is independent of the type of electrode (roughness factor). Conversely, the CO yield does depend on the type of electrode. At the high current density, both H_2 and CO production depend on the electrode parameters. The highest CO yield (> 80%) is obtained using a commercially available etched silver foam at 150 mA/cm$^2_{geo}$.

1. Introduction

One of the few opportunities for building a commercially viable process for making chemicals from CO_2 is by conversion of concentrated CO_2 emissions from industrial flue gases, including biogenic CO_2.[1–4] Depending on the industrial plant, flue gas CO_2 concentrations range between 8%–9% for oil refining, 14%–33% for cement manufacturing, and 20%–44% for iron and steel production.[5,6] The most straightforward electrochemical option for utilizing this CO_2 is by reducing it to CO, which can then be combined with hydrogen, green or otherwise, to form syngas. In practice, this reduction half-reaction is always coupled to an oxidation, where water is the most common counter-reactant (Figure 1). Note that by decoupling the CO_2-to-CO and the CO-to-chemicals stages, one can achieve a larger product scope.[7]

When both the source of CO_2 and the CO application are at high pressures, a high-pressure CO_2R technology has an advantage, as it avoids costly depressurising/repressurising cycles. Another benefit of the high pressure is the increased solubility of CO_2 in the aqueous electrolyte (organic solvents such as acetonitrile are possible alternatives,[8–11] but they also complicate the system further).[12–15] At ambient pressure, the extremely low CO_2 solubility results in negligible CO_2 conversions. Gas diffusion electrodes (GDEs) can be used to increase the current density, but these electrodes experience flooding at long operation times, causing long-term stability problems.[16–18] There are few examples of systems that rely on pressurised, concentrated CO_2 in aqueous electrolytes.[19–21] However, realising such a process on industrial scale requires active, selective and above all stable electrodes.[22]

Solid metal silver electrodes are both mechanically and chemically stable. Moreover, they can be recycled, increasing their environmental and economic appeal. The electrochemical CO_2 reduction reaction (CO_2RR), using silver electrodes in aqueous media, produces mainly CO with H_2 and formic acid as by-products.[23,24] CO_2-to-CO is a two-electron reduction (reaction pathway shown in Figure 2).[25–28] First, CO_2 adsorbs on the surface to form *COOH. This can be either as a proton-coupled electron transfer (PCET) to directly form *COOH (Equation 1), or in a decoupled pathway. In the latter, CO_2 binds to the surface and accepts an electron to form a CO_2 radical anion (Equation 2) before reacting with a proton to form the carboxyl intermediate (Equation 3). After *COOH is formed, the intermediate reacts with another proton and electron, giving *CO and water (Equation 4). Finally, the CO desorbs from the surface (Equation 5). Formic acid can form when the CO_2 molecule adsorbs via its oxygen (Figure S1):[27]

$$CO_2\,(g) + {}^{*} + H^+\,(aq) + e^- \rightleftharpoons {}^{*}COOH \quad (1)$$

$$CO_2\,(g) + {}^{*} + e^- \rightleftharpoons {*}COO^- \quad (2)$$

$${}^{*}COO^- + H^+\,(aq) \rightleftharpoons {}^{*}COOH \quad (3)$$

$${}^{*}COOH + H^+\,(aq) + e^- \rightleftharpoons {}^{*}CO + H_2O\,(l) \quad (4)$$

[a] N. I. Watson, C. von Quadt, G. Rothenberg
Van 't Hoff Institute for Molecular Sciences, University of Amsterdam, Science Park 904, 1098XH, Amsterdam, The Netherlands
E-mail: g.rothenberg@uva.nl

[b] N. I. Watson, C. von Quadt, S. Molodtsov, L. Balk, B. van den Bosch
VOLTA Department, Avantium Chemicals, Matrix Building 6, Science Park 408, 1098XH, Amsterdam, The Netherlands

Supporting information for this article is available on the WWW under https://doi.org/10.1002/cctc.202501122

© 2025 The Author(s). ChemCatChem published by Wiley-VCH GmbH. This is an open access article under the terms of the Creative Commons Attribution-NonCommercial License, which permits use, distribution and reproduction in any medium, provided the original work is properly cited and is not used for commercial purposes.

© 2025 The Author(s). ChemCatChem published by Wiley-VCH GmbH

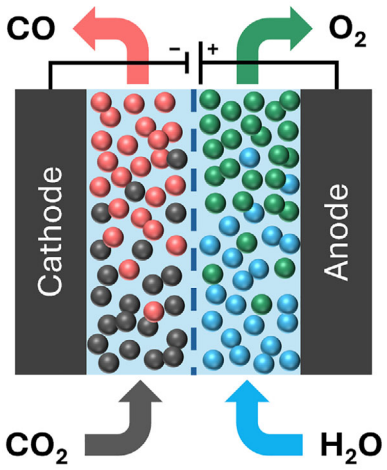

Figure 1. Cartoon of a simplified CO_2 electrolyzer, showing the simultaneous conversion of CO_2 (black spheres) to CO (red) at the cathode and water (light blue spheres) to oxygen (green) at the anode.

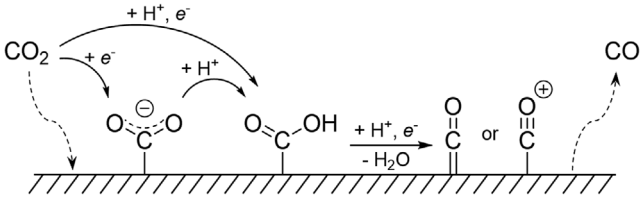

Figure 2. Reaction pathways of CO_2-to-CO electroreduction on a surface in aqueous media.[25–28]

$$^{*}CO \rightleftharpoons CO\,(g) + {}^{*} \tag{5}$$

Competing with the CO_2RR is the hydrogen evolution reaction (HER) (Figure S2). This is also a two-electron reduction, but here either direct proton reduction or water reduction takes place. In acidic media, direct proton reduction takes place to form H_2 (Equation 6).[29,30] Under alkaline conditions, water is reduced (Equation 7). The two processes, HER and CO_2RR, both require protons to be close to the electrode. But they are distinct in the sense that the HER does not require the presence of CO_2 at the electrode:

$$2H^{+} + 2e^{-} \rightleftharpoons H_2 \tag{6}$$

$$2H_2O + 2e^{-} \rightleftharpoons H_2 + OH^{-} \tag{7}$$

In this paper, we study the electrochemical reduction of CO_2 to CO, coupled to water oxidation, under industrially relevant conditions. We use commercially available silver electrodes with different modifications, and examine the parameters that govern the product selectivity and the competition with the hydrogen evolution reaction.

2. Results and Discussion

2.1. Electrode Designation and Analysis

We used three commercial Ag foam electrodes for the high pressure electrochemical reduction of CO_2: a standard silver foam (Ag_{foam}), an etched foam (Ag_{etched}) and a nanoparticle functionalised foam (Ag_{NP}). The foams were analysed by optical microscopy imaging, X-ray diffraction (XRD) and cyclic voltammetry (CV). Figure 3 shows optical microscopy images of the electrodes at 50X and 500X magnification. The three foams are similar, but Ag_{etched} and Ag_{NP} show a rougher surface compared to Ag_{foam}. Where Ag_{foam} (Figure 3A) has a shiny, uniform surface, Ag_{etched} (Figure 3B) and Ag_{NP} (Figure 3C) have a slightly matte finish. Moreover, Ag_{NP} has silver particles protruding from the surface, indicating a higher level of surface roughness.

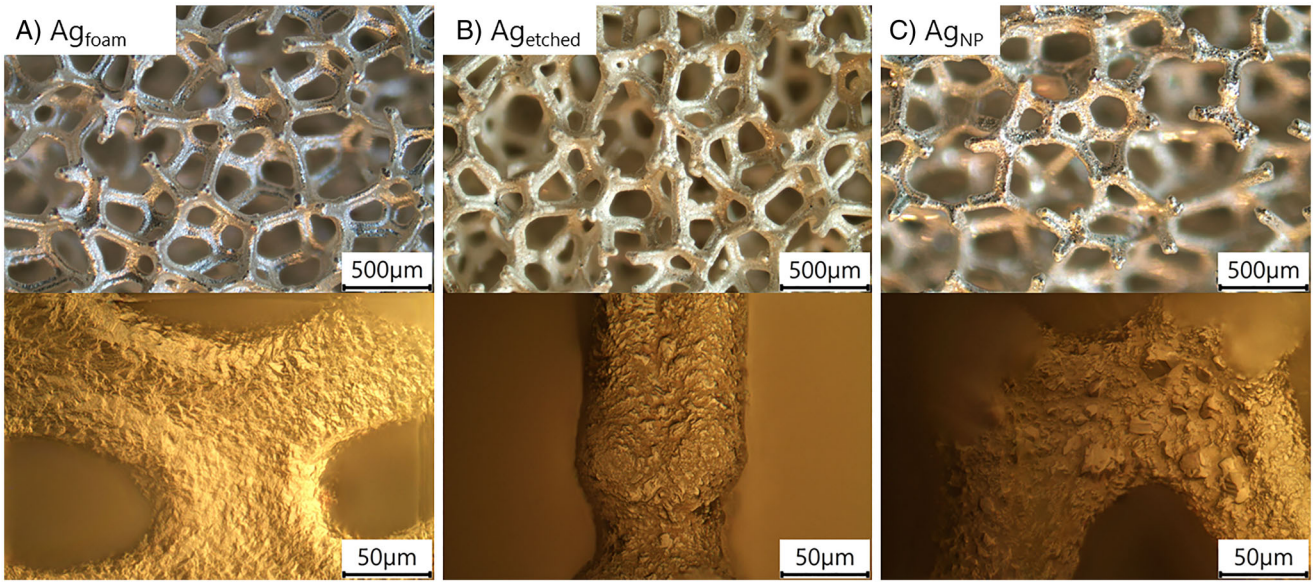

Figure 3. Optical microscopy photos at 50× and 500× magnification of commercial A) Ag_{foam}, B) Ag_{etched}, and C) Ag_{NP}.

© 2025 The Author(s). *ChemCatChem* published by Wiley-VCH GmbH

18673899, 2025, 21, Downloaded from https://chemistry-europe.onlinelibrary.wiley.com/doi/10.1002/cctc.202501122 by Universidad De Valladolid, Wiley Online Library on [26/11/2025]. See the Terms and Conditions (https://onlinelibrary.wiley.com/terms-and-conditions) on Wiley Online Library for rules of use; OA articles are governed by the applicable Creative Commons License

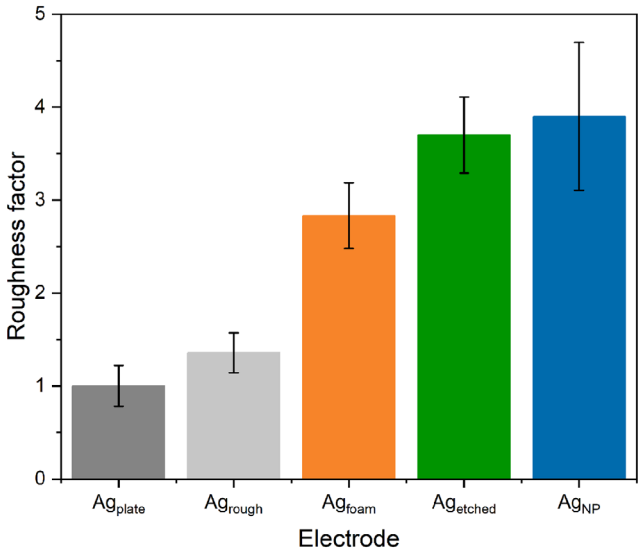

Figure 4. Roughness factors of the silver electrodes calculated from ECSA measurements by integration of surface silver reduction events.

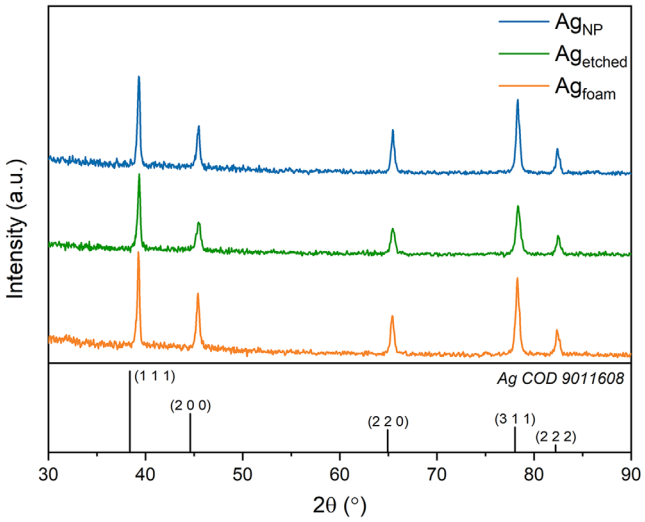

Figure 5. X-ray diffractograms of Ag_{foam}, Ag_{etched}, and Ag_{NP} measured between 30° and 90° at a rotational speed of 2.5 °/min. All three Ag foams show peaks corresponding to Ag (111), (200), (220), (311), and (222) facets.

To compare this observed surface roughness, we determined the electrochemically active surface area (ECSA) for each electrode. The ECSA and the resulting roughness factors were calculated by integration of surface silver reduction events. The determination of the ECSA using cyclic voltammetry is discussed elsewhere.[31,32] Specifically, we use the reduction of Ag^+ to metallic silver ($Ag^+ + e^- \rightleftharpoons Ag^0$) to determine the roughness factors. Figure 4 shows the roughness factors of the three foam electrodes and two additional silver plate ones, a pristine silver plate (Ag_{plate}), and a mechanically roughened plate (Ag_{rough}). Each plate electrode is a 2 × 1 cm rectangle, the same nominal measure as the foam samples. The two plate electrodes were included to validate the chosen ECSA approach. Indeed, we find that the ECSA increases as expected: $Ag_{plate} < Ag_{rough} < Ag_{foam} < Ag_{etched} < Ag_{NP}$ (the results are averages of triplicate measurements, see also the peak integrations used to obtain the roughness factors in Figures S3–S7).

X-ray diffractograms of the Ag foam electrodes are shown in Figure 5. All three electrodes show the characteristic peaks of polycrystalline silver. Specifically, we see peaks at 39.3°, 45.5°, 65.4°, 78.3°, and 82.4°, corresponding to silver (111), (200), (220), (311), and (222) facets, respectively. The electrodes have nearly identical XRD patterns and peak intensity ratios. This is expected, as the bulk of these materials is the same, namely silver. The slight differences in peak intensities within a sample could originate from measuring a foam material, where the sample packing is not ideal. They could also originate from the surface modifications (etching of the material or deposition of silver nanoparticles). However, this is less likely because the modifications are not designed to expose a specific facet.

2.2. Performance in CO_2RR

During electrolysis, gas samples were taken from the reactor headspace and analysed by gas chromatography. Helium (He) was used as an internal standard for quantifying the different components in the gas stream. Figure 6 shows an example of the different cathodic gases and CO_2 for a 22 + h electrolysis using Ag_{foam} at both 150 and 300 mA/cm$^2_{geo}$. Note that these reactions were run in a continuous system, where CO_2 was fed continuously to maintain the saturation concentration in the electrolyte, and no reference electrode was used. Therefore, the cathodic gas stream has an excess of CO_2 (36 mL/min). For the lower current density electrolysis (Figure 6A), CO and H_2 were measured at an average of 1.73 and 0.08 mL/min, respectively. For the electrolysis at 300 mA/cm$^2_{geo}$ (Figure 6B), the measured flows were 2.14 and 0.35 mL/min, respectively.

From the cathodic gas flows, we calculated the Faraday yields of CO and H_2. Figure 7 shows an example of the Faraday yield (FY) progress over time (specifically, Figure 7A shows the electrolysis at 150 mA/cm$^2_{geo}$ and Figure 7B shows the yields at 300 mA/cm$^2_{geo}$). For both runs, the FY toward CO is higher than for H_2, and the total FY for the lower current density run is higher. During all these electrolysis runs, the electrodes maintained their activity.

To compare the FY between runs and for the various silver electrodes, the average FY was calculated (Figure 8). Generally, the total FY is lower for the runs at 300 mA/cm$^2_{geo}$, except for Ag_{plate}, where the total yield increases. For all the electrodes, the CO Faraday yield decreases when changing from 150 to 300 mA/cm$^2_{geo}$ while the H_2 yield increases. Specifically, the CO drops with 76% for Ag_{plate}, 37% for Ag_{foam}, 38% for Ag_{etched}, and 41% for Ag_{NP}. Meanwhile, the H_2 yield increases for Ag_{plate} by 5.5X, and for Ag_{foam}, Ag_{etched}, and Ag_{NP}, it's at least doubled. The highest selectivity towards CO was obtained using Ag_{etched} with a FY of 82.6% at 150 mA/cm$^2_{geo}$. In contrast, the lowest CO FY was obtained using Ag_{plate} at 300 mA/cm$^2_{geo}$ at 7.9%. The drop in CO selectivity and increase in H_2 production when doubling the applied current density show that HER is outcompeting CO_2RR.

Whilst overcoming the low CO_2 solubility challenge by pressurising the system, the concentration of CO_2 in the double layer

© 2025 The Author(s). *ChemCatChem* published by Wiley-VCH GmbH

18673899, 2025, 21, Downloaded from https://chemistry-europe.onlinelibrary.wiley.com/doi/10.1002/cctc.202501122 by Universidad De Valladolid, Wiley Online Library on [26/11/2025]. See the Terms and Conditions (https://onlinelibrary.wiley.com/terms-and-conditions) on Wiley Online Library for rules of use; OA articles are governed by the applicable Creative Commons License

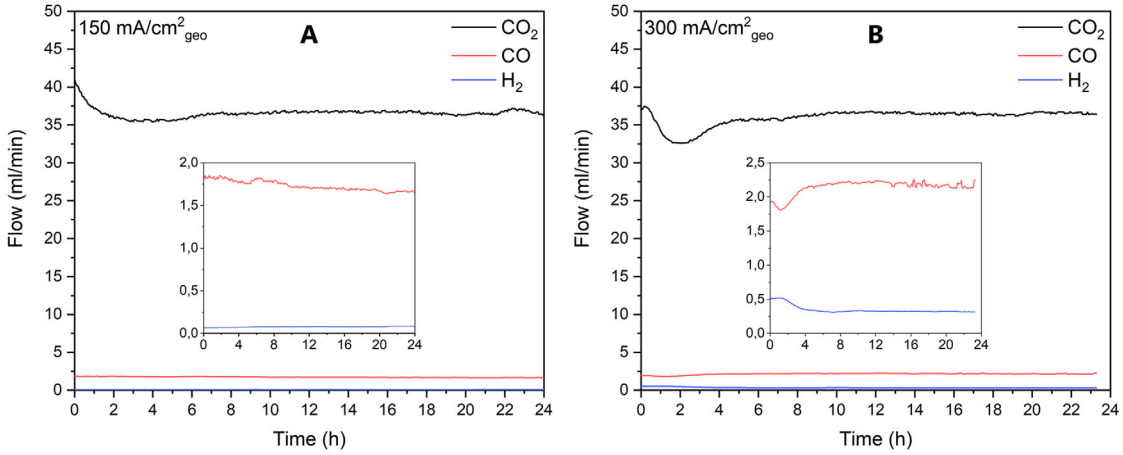

Figure 6. Cathodic gas flows from a 22 + h electrolysis with Ag_{foam} at A) 150 mA/cm$^2_{geo}$ and B) 300 mA/cm$^2_{geo}$.

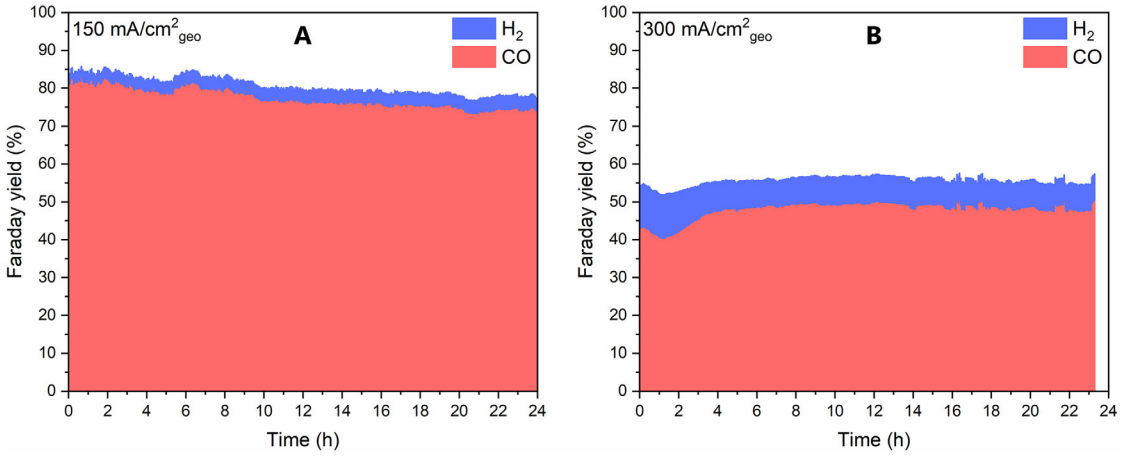

Figure 7. Time-dependent Faraday yield of gaseous CO_2R electrolysis products using Ag_{foam} at A) 150 mA/cm$^2_{geo}$ and B) 300 mA/cm$^2_{geo}$.

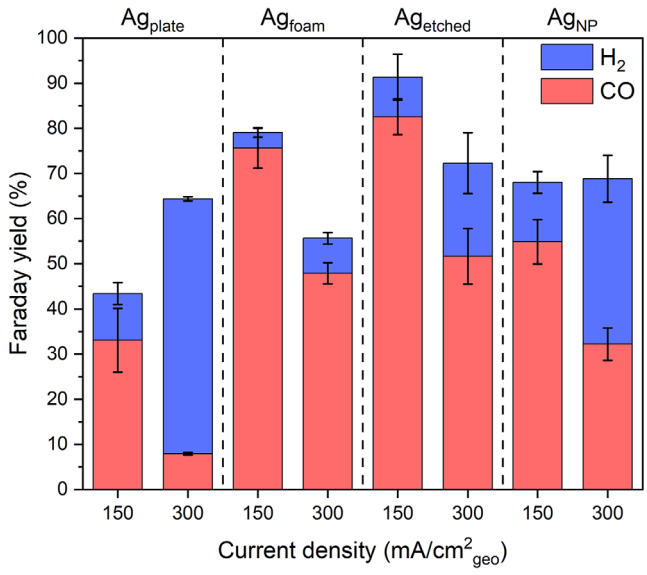

Figure 8. Faraday yield of gaseous CO_2R products of the different electrodes at 150 mA/cm$^2_{geo}$ and 300 mA/cm$^2_{geo}$.

is still limited by mass transport at these high current densities. As this is an aqueous system, instead of seeing predominantly CO_2RR, HER becomes more prominent at higher current densities. Note that the Faraday yields do not add up to 100%. This is because only gaseous products could be detected during electrolysis, and only CO and H_2 were screened. A comparison of the CO Faraday yield between different pressures (15, 30, and 45 bar) at both 50 and 250 mA/cm$^2_{geo}$ is shown in Figure S9. We see that in the 50 mA/cm$^2_{geo}$ experiments, the system is not mass transport limited, as comparable CO Faraday yields are obtained. Whereas this is not the case in the 250 mA/cm$^2_{geo}$ system. There, the CO yield is improved with increasing pressure. Another possible product using silver electrodes is formate.[33–35] Elsewhere, it was reported that CO can be reduced electrochemically under high pressure to ethanol and propanol using silver electrodes.[36] But as our electrolysis took place in a semi-separated batch system, such products, if any, would have been oxidised at the anode. We label this system as "semi-separated", as a gap was left at the bottom of the membrane holder to counteract a shift in electrolyte levels for long runs, thus enabling mixing and diffusion of liquid products (see photos and schematics in Figure S10).

© 2025 The Author(s). *ChemCatChem* published by Wiley-VCH GmbH

18673899, 2025, 21, Downloaded from https://chemistry-europe.onlinelibrary.wiley.com/doi/10.1002/cctc.202501122 by Universidad De Valladolid, Wiley Online Library on [26/11/2025]. See the Terms and Conditions (https://onlinelibrary.wiley.com/terms-and-conditions) on Wiley Online Library for rules of use; OA articles are governed by the applicable Creative Commons License

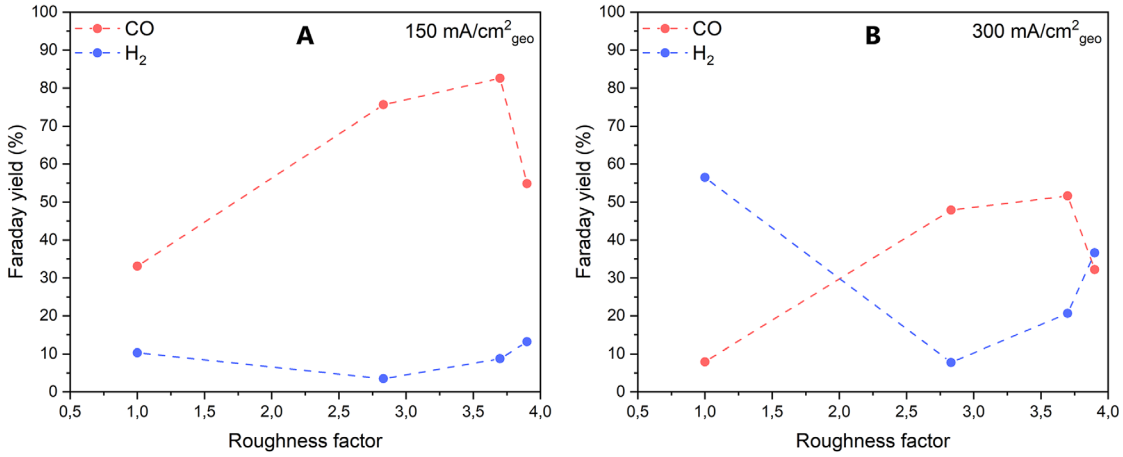

Figure 9. Faraday yield of gaseous CO_2R products dependence on surface roughness at A) 150 mA/cm$^2_{geo}$ and B) 300 mA/cm$^2_{geo}$. Note that although the yields in (B) look like they mirror each other, the values for CO and H_2 were in fact calculated separately, based on their GC peak areas.

Analysis of the electrolyte post-electrolysis showed only trace amounts of formate.

Because the selectivity to CO and H_2 depends on the applied current, we also studied it against the surface roughness. Figure 9A,B show the FY for CO and H_2 at 150 mA/cm$^2_{geo}$ and 300 mA/cm$^2_{geo}$, respectively. At 150 mA/cm$^2_{geo}$, the selectivity for H_2 does not depend on the surface roughness – all electrodes have a yield $<$ 3% hydrogen. In contrast, the CO selectivity varies between 33% and 83%, depending on the electrode. Surprisingly, we see a difference between the three foam electrodes: where Ag_{foam} and Ag_{etched} show a similar high FY, Ag_{NP} has a much lower CO yield at 55%. This suggests that increasing the surface area does not result in higher CO yields at 150 mA/cm$^2_{geo}$. The same comparison was done for the Faraday yields at 300 mA/cm$^2_{geo}$ (Figure 9B). Here, both the CO and H_2 yields change significantly with a change in surface roughness.

The fact that hydrogen production on the foam electrodes becomes dependent on the surface area at 300 mA/cm$^2_{geo}$ reflects the much higher concentration of protons in the double layer. The system can fulfil the high current demand by performing more HER when the CO_2 concentration at the double layer is depleted (Figure 10). As the ESCA increases, the overall observed FY remains between 55% and 70%, showing that the formation of other CO_2RR products, such as formate, remains constant. The higher FY for the pristine plate electrode may reflect the lower affinity of CO_2 to the smooth electrode, which reduces the chance of both CO and formate formation.

3. Conclusions

High-pressure electrochemical reduction of CO_2 to syngas is possible using commercial silver foam electrodes. Moreover, the stability and scalability of the system open opportunities for real-life applications. CO Faraday yields in such systems can exceed 80%, and the competing hydrogen evolution reaction can be suppressed by tuning the applied current. The trade-off between

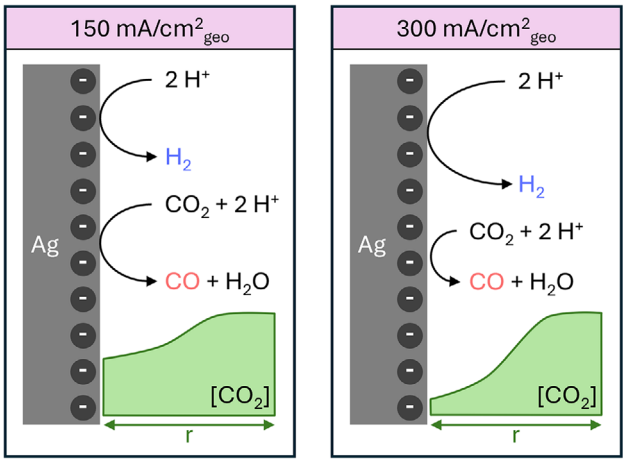

Figure 10. Schematic of the CO_2RR and the HER at the surface, where the CO_2 concentration (green) near the surface is depleted at the higher current density. Here, "r" denotes the distance between the double layer and the bulk electrolyte.

CO and formate products has been shown to depend on the reaction pressure.[24] Yet we also show that while the CO_2 reduction reaction always depends on the electrode surface area, the HER only depends on the area at high current densities. Thus, the current density is the most important single factor that governs the CO selectivity.

The past decade has seen an explosion in the number of studies reporting on electrochemical CO_2 reduction. However, most of these studies run under model conditions, which means low pressures. The main reason for this is that building and maintaining high-pressure electrochemical laboratory setups is difficult and costly. Low-pressure studies can give valuable fundamental information about electrochemical reactions. Yet as we show here, there is rarely a 1:1 relationship between the reaction parameters under "laboratory conditions" and "industrial conditions".[37] Running electrochemical reactions under industrially relevant conditions is crucial if one wants to obtain industrially relevant results.

© 2025 The Author(s). *ChemCatChem* published by Wiley-VCH GmbH

18673899, 2025, 21, Downloaded from https://chemistry-europe.onlinelibrary.wiley.com/doi/10.1002/cctc.202501122 by Universidad De Valladolid, Wiley Online Library on [26/11/2025]. See the Terms and Conditions (https://onlinelibrary.wiley.com/terms-and-conditions) on Wiley Online Library for rules of use; OA articles are governed by the applicable Creative Commons License

18673899, 2025, 21, Downloaded from https://chemistry-europe.onlinelibrary.wiley.com/doi/10.1002/cctc.202501122 by Universidad De Valladolid, Wiley Online Library on [26/11/2025]. See the Terms and Conditions (https://onlinelibrary.wiley.com/terms-and-conditions) on Wiley Online Library for rules of use; OA articles are governed by the applicable Creative Commons License

4. Experimental Section

4.1. Materials and Instrumentation

Unless stated otherwise, all chemicals were obtained from commercial suppliers and used as received. Silver foam electrodes were obtained from Alantum Europe, and silver plate electrodes (0.1 mm, > 99.99%) were purchased from Alfa Aesar. Acetone (> 99%) and ethanol (96.2%) were sourced from VWR Chemicals. Hydrochloric acid (37%) was obtained from Fisher Scientific, potassium hydroxide (85%) from Thermo Scientific, and potassium bicarbonate (> 99.95%) from Sigma Aldrich. CO_2 (99.99%), He (99.99%), and Ar (99.99%) were all supplied by Messer. N_2 (99.99%) was supplied by Linde Gas. Mechanical roughening of plate electrodes was performed using P120 grid sandpaper. Millipore Milli-Q purified water was used for all solutions in this work.

Cyclic voltammograms were taken in an undivided three-electrode cell, equipped with a graphite rod (Sigma-Aldrich) counter electrode and an Ag/AgCl (Mengel Engineering) reference. For these experiments, a Multi Autolab/M204 potentiostat (Metrohm) was used. Results were not compensated for the ohmic drop. Reported potentials were converted to RHE according to Equation (8):

$$E_{RHE} = E_{Ag/AgCl(KClsat)} + E^{\circ}{}_{Ag/AgCl(KClsat)} + 0.059 \times pH \quad (8)$$

The high-pressure electrolysis experiments were performed in a semi-separated Parr autoclave (SS 316) equipped with two electrode ports and a Nafion 117 (Ion Power, 6 × 4.5 cm) membrane. Here, a custom-made membrane holder was used, where the electrode distance was fixed at 15 mm from the CEM. Silver electrodes were attached to the holder using Teflon tape, and the electrical connection was made using Ag wire. The counter electrode used was a Ti mesh Ir-MMO (Magneto Special Anodes) and was connected by Ti wire. Both electrical connections are shielded from the electrolyte with PTFE tape. To prevent cathodic volume increase over time, a gap at the bottom of the holder was left to allow for liquid flow between the compartments, hence a semi-separated cell. Gases were fed to the autoclave using Bronkhorst mass flow controllers (MFCs). CO_2 was bubbled in excess (15X) at the cathodic compartment using a plastic sparger. Helium was mixed in as an internal standard for GC analysis. CO_2 was fed at 50 mL/min and He at 1 mL/min (see also a schematic and piping and instrumentation diagram in the Supporting Information).

Optical microscope images were obtained using a Delphi-X Observer equipped with a sCMEX-20 camera using ImageFocusAlpha software. X-ray diffraction (XRD) was measured on a MiniFlex II diffractometer (Rikagu) with Ni-filtered CuKα radiation at 30 kV. Diffraction patterns were taken between 30° and 9° (2θ) at a scan speed of 2.5°/min with a 0.05° step size. Gas chromatography (GC) was used to analyze the gaseous products on a Varian CP-4900 4-channel Micro Gas Chromatograph. Argon served as a carrier gas, and helium was used as an internal standard. The product gas mix was depressurised to atmospheric pressure using an Equilibar pressure regulator and dried over a column before GC analysis.

4.2. Procedures

Electrode preparation: Silver foam and silver plate electrodes were cut into 1 × 2.5 cm pieces and mechanically roughened where needed. The electrodes were cleaned by sequential sonication in 6 M HCl for 30 min, followed by sonication in acetone, ethanol, and water for 15 min each. In between each sonication step, the pieces were rinsed with water. The clean Ag electrodes were dried overnight at room temperature.

Cyclic voltammetry (CV): CVs to determine the ECSA by Ag^{+}/Ag^{0} transition integration were taken from –1.0 V and 1.0 V versus Ag/AgCl in N_2-degassed 1 M KOH. A total of three cycles was recorded per electrode at a scan speed of 50 mV/s.

Electrolysis: Electrolysis experiments were performed at 30 bar, 5 °C, and at an applied current density of 150 $mA/cm^2{}_{geo}$ or 300 $mA/cm^2{}_{geo}$. All experiments were conducted in a 0.5 M $KHCO_3$ electrolyte, which was stirred at 600 rpm. The applied current was held for 4.5–25 h, depending on the run.

Acknowledgments

The CO2SMOS project has received funding from the European Union's Horizon 2020 research and innovation programme under grant agreement No 101000790.

Conflict of Interests

The authors declare no conflict of interest.

Data Availability Statement

The data that support the findings of this study are available from the corresponding author upon reasonable request.

Keywords: Electrocatalysis · Flue gases · Hydrogen evolution · Industrial effluents · Silver electrodes

[1] O. Y. Abdelaziz, W. M. Hosny, M. A. Gadalla, F. H. Ashour, I. A. Ashour, C. P. Hulteberg, *J. CO_2 Util.* **2017**, *21*, 52–63.
[2] G. Rothenberg, *Sust. Chem. Clim. Action* **2023**, *2*, 100012.
[3] L. F. Bobadilla, J. M. Riesco-García, G. Penelás-Pérez, A. Urakawa, *J. CO_2 Util.* **2016**, *14*, 106–111.
[4] J. W. Maina, J. M. Pringle, J. M. Razal, S. Nunes, L. Vega, F. Gallucci, L. F. Dumée, *ChemSusChem* **2021**, *14*, 1805–1820.
[5] D. R. Van Puyvelde, *Energy Procedia* **2009**, *1*, 109–116.
[6] M. Songolzadeh, M. Soleimani, M. Takht Ravanchi, R. Songolzadeh, *Sci. World J.* **2014**, *2014*, 1–34.
[7] P. Papangelakis, C. P. O'Brien, A. Shayesteh Zeraati, S. Liu, A. Paik, V. Nelson, S. Park, Y. C. Xiao, R. Dorakhan, P. Sun, J. Wu, C. M. Gabardo, N. Wang, R. K. Miao, E. H. Sargent, D. Sinton, *Nat. Commun.* **2025**, *16*, 4969.
[8] C. Deacon-Price, A. H. M. da Silva, C. S. Santana, M. T. M. Koper, A. C. Garcia, *J. Phys. Chem. C* **2023**, *127*, 14518–14527.
[9] C. Deacon-Price, N. Chen, A. Lal, P. Broersen, E. J. Meijer, A. C. Garcia, *ChemCatChem* **2025**, *17*, e202401332.
[10] M. C. Figueiredo, I. Ledezma-Yanez, M. T. M. Koper, *ACS Catal.* **2016**, *6*, 2382–2392.
[11] P. B. Joshi, N. Karki, A. J. Wilson, *ACS Energy Lett.* **2022**, *7*, 602–609.
[12] R. Wiebe, V. L. Gaddy, *J. Am. Chem. Soc.* **1940**, *62*, 815–817.
[13] R. Wiebe, V. L. Gaddy, *J. Am. Chem. Soc.* **1939**, *61*, 315–318.
[14] Z. Duan, R. Sun, *Chem. Geol.* **2003**, *193*, 257–271.
[15] A. Hemmati-Sarapardeh, M. N. Amar, M. R. Soltanian, Z. Dai, X. Zhang, *Energy Fuels* **2020**, *34*, 4761–4776.
[16] K. Yang, R. Kas, W. A. Smith, T. Burdyny, *ACS Energy Lett.* **2021**, *6*, 33–40.
[17] T. Zhang, Z. Li, X. Lyu, J. Raj, G. Zhang, H. Kim, X. Wang, S. Chae, L. Lemen, V. N. Shanov, J. Wu, *J. Electrochem. Soc.* **2022**, *169*, 104506.
[18] P. Tiwari, G. Tsekouras, G. F. Swiegers, G. G. Wallace, *ACS Appl. Mater. Interfaces* **2018**, *10*, 28176–28186.
[19] F. Proietto, F. Berche, A. Galia, O. Scialdone, *J. Appl. Electrochem.* **2021**, *51*, 267–282.

© 2025 The Author(s). *ChemCatChem* published by Wiley-VCH GmbH

[20] A. R. T. Morrison, N. Girichandran, Q. Wols, R. Kortlever, *J. Appl. Electrochem.* **2023**, *23*, 2321–2330.
[21] S. Lamaison, D. Wakerley, J. Blanchard, D. Montero, G. Rousse, D. Mercier, P. Marcus, D. Taverna, D. Giaume, V. Mougel, M. Fontecave, *Joule* **2020**, *4*, 395–406.
[22] D. F. Bruggeman, G. Rothenberg, A. C. Garcia, *Nat. Commun.* **2024**, *15*, 9207.
[23] S. Nitopi, E. Bertheussen, S. B. Scott, X. Liu, A. K. Engstfeld, S. Horch, B. Seger, I. E. L. Stephens, K. Chan, C. Hahn, J. K. Nørskov, T. F. Jaramillo, I. Chorkendorff, *Chem. Rev.* **2019**, *119*, 7610–7672.
[24] L. Huang, G. Gao, C. Yang, X.-Y. Li, R. K. Miao, Y. Xue, K. Xie, P. Ou, C. T. Yavuz, Y. Han, G. Magnotti, D. Sinton, E. H. Sargent, X. Lu, *Nat. Commun.* **2023**, *14*, 2958.
[25] B. Seger, G. Kastlunger, A. Bagger, S. B. Scott, *ACS Energy Lett.* **2025**, *10*, 2212–2227.
[26] N. J. Firet, W. A. Smith, *ACS Catal.* **2017**, *7*, 606–612.
[27] Z. Sun, T. Ma, H. Tao, Q. Fan, B. Han, *Chem* **2017**, *3*, 560–587.
[28] G. M. Tomboc, S. Choi, T. Kwon, Y. J. Hwang, K. Lee, *Adv. Mater.* **2020**, *32*, 1908398.
[29] N. Dubouis, A. Grimaud, *Chem. Sci.* **2019**, *10*, 9165–9181.
[30] J. Li, Z. Jing, H. Bai, Z. Chen, A. I. Osman, M. Farghali, D. W. Rooney, P.-S. Yap, *Environ. Chem. Lett.* **2023**, *21*, 2583–2617.
[31] R. Martínez-Hincapié, J. Wegner, M. U. Anwar, A. Raza-Khan, S. Franzka, S. Kleszczynski, V. Čolić, *Electrochim. Acta* **2024**, *476*, 143663.
[32] C. Wei, S. Sun, D. Mandler, X. Wang, S. Z. Qiao, Z. J. Xu, *Chem. Soc. Rev.* **2019**, *48*, 2518–2534.
[33] N. Hoshi, M. Kato, Y. Hori, *J. Electroanal. Chem.* **1997**, *440*, 283–286.
[34] X. Zhu, J. Huang, M. Eikerling, *ACS Catal.* **2021**, *11*, 14521–14532.
[35] T. Hatsukade, K. P. Kuhl, E. R. Cave, D. N. Abram, T. F. Jaramillo, *Phys. Chem. Chem. Phys.* **2014**, *16*, 13814–13819.
[36] S. J. Raaijman, M. P. Schellekens, P. J. Corbett, M. T. M. Koper, *Angew. Chem., Int. Ed.* **2021**, *60*, 21732–21736.
[37] L. Li, P. C. M. Laan, X. Yan, X. Cao, M. J. Mekkering, K. Zhao, L. Ke, X. Jiang, X. Wu, L. Li, L. Xue, Z. Wang, G. Rothenberg, N. Yan, *Adv. Sci.* **2023**, *10*, 2206180.

Manuscript received: September 3, 2025
Accepted manuscript online: September 5, 2025
Version of record online: September 17, 2025

© 2025 The Author(s). *ChemCatChem* published by Wiley-VCH GmbH

18673899, 2025, 21, Downloaded from https://chemistry-europe.onlinelibrary.wiley.com/doi/10.1002/cctc.202501122 by Universidad De Valladolid, Wiley Online Library on [26/11/2025]. See the Terms and Conditions (https://onlinelibrary.wiley.com/terms-and-conditions) on Wiley Online Library for rules of use; OA articles are governed by the applicable Creative Commons License